2021

Development and Evaluation of Low-Cost CO2 Sensors for Buildings

Zachary A. Siefker
Purdue University

Abhi R. Boyina
Purdue University

Xikang Zhao
Purdue University

John N. Hodul
Purdue University

James E. Braun
Purdue University

See next page for additional authors

Development and Evaluation of Low-Cost CO_2 Sensors for Buildings

Zachary A. Siefker[1,2], Abhi Boyina[1,2], Xikang Zhao[3], John N. Hodul[2,4], James E. Braun[1,2], George T.-C. Chiu[1,2], Bryan W. Boudouris[3,4], Jeffrey F. Rhoads[1,2*]

[1] School of Mechanical Engineering
[2] Ray W. Herrick Laboratories
[3] Charles D. Davidson School of Chemical Engineering
[4] Department of Chemistry
Purdue University, West Lafayette, IN 47907

* Corresponding Author

ABSTRACT

There is a significant opportunity to improve building energy efficiency and indoor environmental quality by accurately monitoring CO_2 levels. However, current CO_2 sensors tend to be expensive or require regular recalibration. This work presents research related to the initial development and evaluation of two novel CO_2 sensors based on chemiresistive and resonant mass sensing techniques. Prototype sensors were assessed in a bench-top test chamber at temperatures, humidity levels, and CO_2 concentrations, typical of indoor environments. Under these conditions, prototype sensors required only 60 mW of power, or less. Further, each sensor was developed to have a footprint of less than 25 mm^2 and a cost of less than $50. Given the relative low cost, small size, and potential for low power consumption, these sensors may serve as an attractive alternative to the commercial CO_2 sensors that are currently available.

1. INTRODUCTION

In the United States, buildings account for nearly 40% of total energy consumption (EIA, 2019). Although the average American spends nearly 90% of their time indoors (EPA, 1989), individual spaces in buildings typically have low or no occupancy much of the time. Thus, there is significant opportunity for reducing energy use by decreasing ventilation rates and adjusting thermostat temperatures according to measured occupancy. One common surrogate measurement for occupancy is a room's carbon dioxide (CO_2) level.

CO_2-based demand controlled ventilation (DCV) offers the possibility of saving energy by reducing building ventilation rates during periods of low occupancy, while also ensuring adequate levels of outdoor air ventilation when necessary. To ensure healthy indoor air, ASHRAE Standard 62.1-2010 suggests maintaining a 700 ppm difference between indoor and outdoor CO_2 concentrations, based on a ventilation rate of 7.5 Lps/person and assuming an occupant activity level of 1.2 MET (ASHRAE, 2010b). In the absence of occupancy data, many systems are designed to provide constant ventilation based on maximum expected occupancy levels. However, studies have shown that CO_2-based DCV can offer up to 44% energy savings as compared to constant-rate ventilation systems (O'Neill et al., 2020). Thus, DCV has the potential to substantially improve building energy efficiency and indoor air quality.

As the Internet of Things (IoT) begins to translate into the buildings sector, new opportunities are arising with the advent of distributed sensing networks to improve building operation (Gunay & Shen, 2017). For example, some studies have shown the possibility of estimating building air leakage by monitoring CO_2 concentration decay patterns (You et al., 2012; Ng & Wen, 2011). Others have suggested using CO_2 sensing for occupancy detection to provide localized comfort control (Candanedo & Feldheim, 2016; Ekwevugbe et al., 2013; Jin et al., 2018). However, the commercial CO_2 sensors that are currently available tend to be costly and difficult to install, especially if implemented as retrofits. Thus, there is a need for low-cost and easily deployable sensors for monitoring indoor CO_2 levels in buildings.

This work presents research related to the initial development and evaluation of low-cost, small, and low-power sensors, suitable for monitoring indoor CO_2 levels. Two different types of sensors are presented that have the potential to perform as well or better than, current commercially available CO_2 sensing technologies. The first is a chemiresistive sensor that uses a carbon nanotube (CNT) thin film in conjunction with a polymer blend of branched polyethylenimine

(PEI) and polyethylene glycol (PEG). The second is a resonant mass sensor functionalized with a similar polymer blend. Prototype sensors were assessed in a bench-top environmental test chamber at boundary points of the 0.5 clo and 1.0 clo comfort zones of ASHRAE standards (ASHRAE, 2010a). Prototype sensors were then benchmarked against commercially available CO_2 sensing technologies.

2. DEVICE FABRICATION AND THEORY OF OPERATION

2.1 Chemiresistive Sensor Fabrication

To prepare the functional polymer blend, PEI (M_n = 10,000 g mol^{-1}) and PEG (M_n = 300 g mol^{-1}) were dissolved in methanol to generate a solution of 1% PEI and 3% PEG. The CNT thin films were prepared by adding 3 mg of CNTs to 3 mL of chlorosulfonic acid and stirring the mixture for 3 days. Then, 20 μL of this solution were sandwiched between two glass slides, and the thin films were generated by manually pressing and sliding across the glass slides, in a manner similar to what has been reported previously (Li et al., 2013). To transfer the thin film, the glass slides were gently placed into water to peel the thin film, and the free-floating films (Figure 1a) were deposited onto pre-patterned electrodes of a printed circuit board (PCB) substrate (Figure 1b). Fabrication of the sensors was completed by drop-casting the functional polymer solution onto the CNT thin films, followed by the removal of methanol by drying for 5 hr in a fume hood.

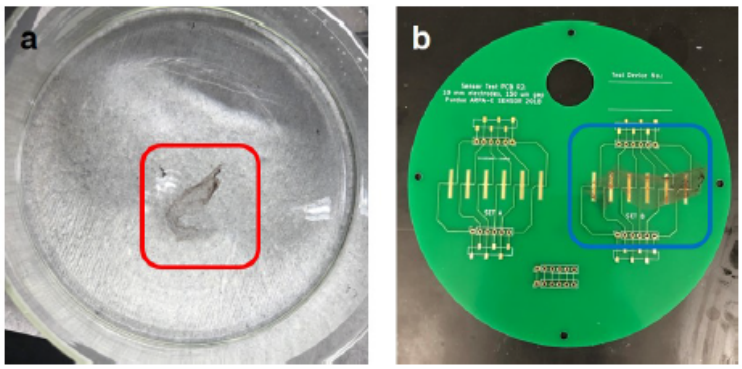

Figure 1: (a) The free-floating CNT film generated after casting a dispersion of the CNTs from a concentrated solution. The CNT film floating on water is highlighted by the red box. (b) The final CNT thin films after they have been laminated atop the pre-fabricated PCB substrates. The devices with the CNT thin films laminated on them are highlighted by the blue box. A separate set of bare electrodes are present, but are intentionally not covered with the CNTs for visual comparison.

2.2 Chemiresistive Sensing Mechanism

A functional mixture of PEI, PEG, and CNTs was utilized for the detection of CO_2. PEI, is a highly branched polymer with several secondary and tertiary amino groups along the polymer backbone. In the mixture, PEI n-dopes the CNTs with its electron negative lone pairs. In the presence of CO_2, the amino groups readily react to form electron deficient ammonium cations, which weakens the n-doping effect. This leads to a change in the carrier concentration within the material. Since this reaction is facilitated by water, PEG is added to serve as a vapor absorbing material.

2.3 Resonant Mass Sensor Fabrication

The resonant mass sensors consisted of a quartz crystal resonator embedded in a Pierce oscillator circuit that utilized a crystal oscillator driver, an inverter, two load capacitors (C_1 = 22 pF and C_2 = 22 pF), a feedback resistor (R_1 = 2 MΩ), and an isolation resistor (R_2 = 510 Ω), as shown in Figure 2a. These circuits were developed with a separate resonator board that connected to the rest of the oscillator circuit via spring pin connectors (Figure 2b). This two-part configuration allowed for easier functionalization of the resonators with the CO_2 sensitive polymer material.

To prepare the functional polymer blend, PEI (M_n = 25 kg mol^{-1}) and PEG (M_n = 100 kg mol^{-1}) were dissolved in methanol to generate a solution of 0.1% PEI and 0.3% PEG. To functionalize each resonator, 1μL of functional material was deposited onto each resonant element using a micro-pipette. The resonator board was then placed in a vacuum oven at 40 ˚C for 8 hours to remove methanol from the solution.

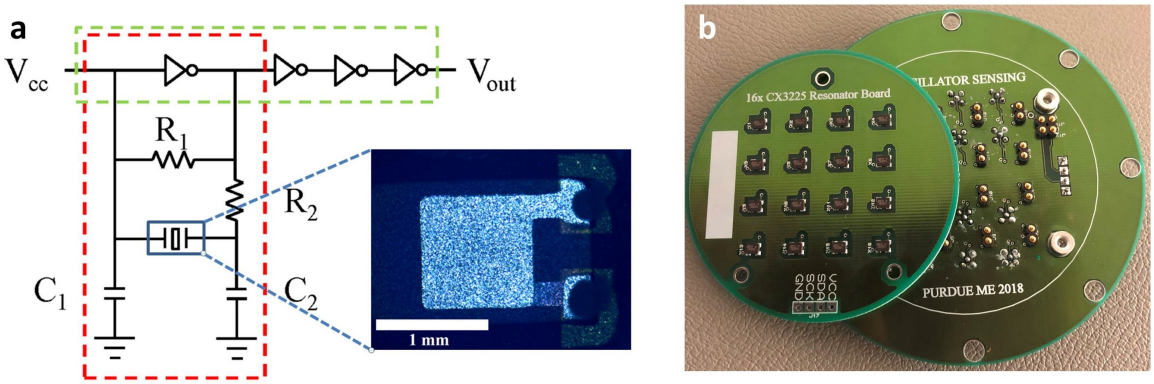

Figure 2: (a) The Pierce oscillator topology used for each resonant mass sensor, with the resonant element shown after the package cap has been removed. (b) A resonant mass sensing system with 16 Pierce oscillators. A resonator board (left) containing 16 resonant elements is shown offset from the instrumentation board (right) which completes the Pierce oscillator circuit.

2.4 Resonant Mass Sensing Mechanism

For bulk acoustic resonators, the added mass due to analyte/sensor interactions induces a shift in the device's resonant frequency. This can be modeled as a simple harmonic oscillator, with the frequency, f, defined as

$$f = \frac{1}{2\pi}\sqrt{\frac{k}{m}} \tag{1}$$

where k is the stiffness and m is the mass of the resonator. Thus, a change in the mass of the resonator, changes its resonant frequency. Similar to the chemiresistive device, a mixture of PEI and PEG was utilized as the CO_2 absorbing layer on the resonator. The sorption of CO_2 in this material results in an increase in the mass of the resonator. Thus, by measuring a given frequency shift, one can measure the presence of CO_2.

3. TESTING PROCEDURE

The bench-top testing system for both the chemiresistive and resonant mass sensors were organized in a similar fashion as seen in Figure 3. The test chamber used for the chemiresistive sensor was a 114 mm diameter and 20 mm tall cylindrical chamber with walls made of aluminum. A 95 mm diameter and 23 mm tall cylindrical aluminum test chamber was used to conduct the resonant mass sensor tests. Thermoelectric coolers (TEC) were attached to the exterior of each test chamber for temperature control of the test environment.

The chamber was equipped with an inline flow distribution system using two gas sources: pure nitrogen and a blend of 1% carbon dioxide balanced with nitrogen. The gas sources were connected to three mass flow controllers (MFC) in parallel. The pure nitrogen gas was connected to two 500 ccm rated MFCs, one of which was connected to a bubbler containing deionized water to introduce humidity to the test chamber. The gas mixture of carbon dioxide and nitrogen was connected to a 40 ccm rated MFC. The output of these three lines converged in a manifold which was connected directly to the testing chamber inlet.

Prior to starting each test, the PCB substrate (chemiresistive sensor) or functionalized resonator board (resonant mass sensor) was secured in the testing chamber. At the start of each test, baseline test conditions were developed by flushing the chamber with nitrogen at a flow rate of 500 ccm, and bringing the chamber to the test-specified temperature and humidity. The test-specified concentrations of CO_2 were then introduced, ensuring the volumetric flow rate was maintained at 500 ccm. For the chemiresistive sensor tests, the resistances were measured using bench-top digital multimeters and a custom measurement program, sampling at a rate of 0.5 Hz. The resonant mass sensor tests utilized frequency counters, implemented in a field programmable gate array (FPGA) within a commercial embedded device. A custom measurement program was designed to count the occurrence of the rising edge of the oscillator output voltage and provided a frequency readout accurate to ±1 Hz.

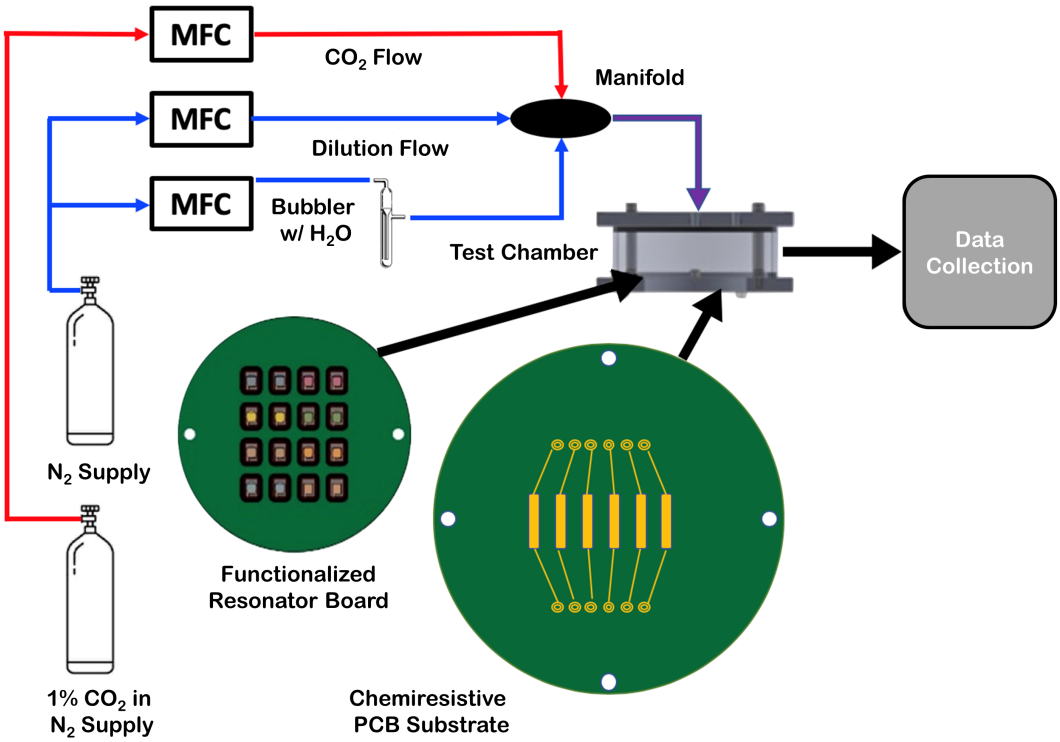

Figure 3: Schematic of gas the distribution system and the bench-top testing setup used to assess the performance of the prototype CO_2 sensors.

Sensor performance was measured at boundary points of the 0.5 clo and 1.0 clo comfort zones stipulated by ANSI/ ASHRAE Standard 55-2010 (ASHRAE, 2010a). These comfort zones approximately span 22–26 °C and from dry air to approximately 80% relative humidity (RH). This region of interest is depicted on the psychrometric chart in Figure 4. Testing was performed near the extremes of each of these regions, as well as near the center, to map sensor performance for typical indoor conditions. Additionally, testing was performed on a background of 400 ppm CO_2, which is approximately the concentration of outdoor air. Higher CO_2 concentrations were introduced, up to 2,000 ppm, to cover the relevant range of expected indoor CO_2 levels.

4. RESULTS AND DISCUSSION

4.1 Chemiresistive Sensor Performance

Figure 5 represents a snapshot of temporal test results for the chemiresistive sensor at each tested environmental condition. As the CO_2 concentration increases, the resistance of the device decreases.The resistance change (blue line) at each CO_2 concentration (red shaded regions) was calculated as

$$\Delta R_0 = \frac{R - R_0}{R_0} \tag{2}$$

where R is the measured electrical resistance, in ohms, and R_0 is the electrical resistance at the start of the temporal data set. The time series data provide a clear indication of sensor responsiveness at each of the environmental test conditions considered. At high humidity conditions, a larger and faster sensor response is demonstrated. At low humidity conditions, a weaker response to CO_2 is evident. More concretely, Figure 6 shows the mean response at each indicated CO_2 concentration as the change in resistance of the device relative to baseline conditions. This relative

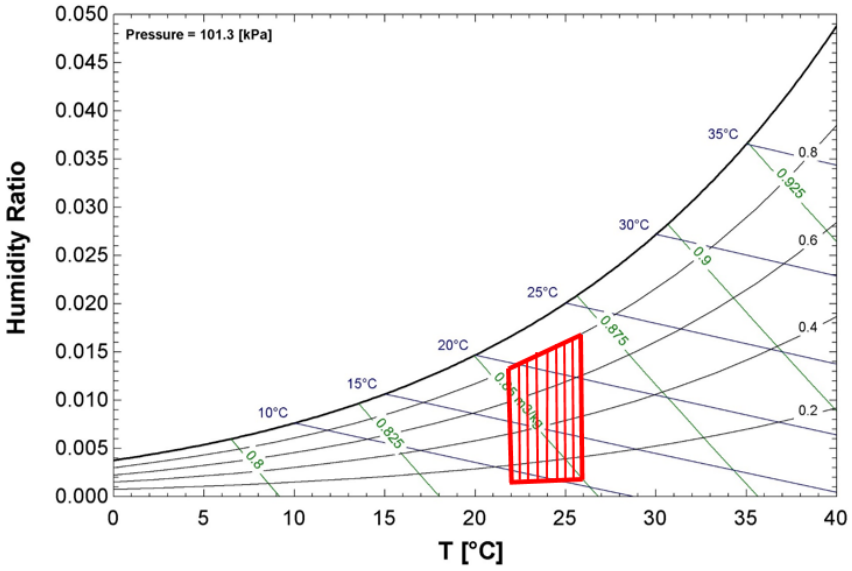

Figure 4: Psychrometric chart highlighting the range of environmental conditions for CO_2 sensor testing. This region spans across the 0.5 clo and 1.0 clo comfort zones stipulated by ANSI/ASHRAE Standard 55-2010 (ASHRAE, 2010a).

resistance change was calculated as

$$\Delta R_b = \frac{R - R_b}{R_b} \tag{3}$$

where R is the measured electrical resistance, in ohms, and R_b is the baseline electrical resistance at the start of each CO_2 pulse. A near-linear trend is present in these data and can be used as a calibration curve for each of the given temperature and RH conditions.

Observing these preliminary data, temperature had a minor influence on the sensor. However, tests across the humidity range show a large difference in the magnitude of the sensor's response to CO_2. In fact, the presence of humidity promotes the sensor's response. Notably, there is a slight signal drift that can be observed in the time series plots. It is hypothesized that this drift is a slight capacitive charging between the electrodes due to the continuous voltage applied during measurement. Thus, real-world applications would require either non-continuous measurement or calibration to the constant drift.

4.2 Resonant Mass Sensor Performance

Figure 7 represents a snapshot of time-series data at each environmental condition for the resonant mass sensor. As the CO_2 concentration increases, the frequency of the device decreases. The frequency change (blue line) at each CO_2 concentration (red shaded regions) was calculated as

$$\Delta f_0 = f - f_0 \tag{4}$$

where f is the measured frequency (Hz) and f_0 is the frequency at the start of the plot. The time series data provide an indication of the sensor's responsiveness, as well as the noise present at each test condition. As evidenced by these plots, a smooth signal is demonstrated at low humidity levels, whereas, higher humidity levels result in a choppier signal as device interaction with water occurs. Further, Figure 8 shows the mean response of the sensor at each indicated CO_2 concentration as the change in frequency relative to baseline conditions. The relative frequency shift was calculated as

$$\Delta f_b = f - f_b \tag{5}$$

where f is the measured frequency and f_b is the baseline frequency at the start of each CO_2 pulse. A near-linear trend is demonstrated in these data, which can serve as a calibration curve for each of the given temperature and RH conditions.

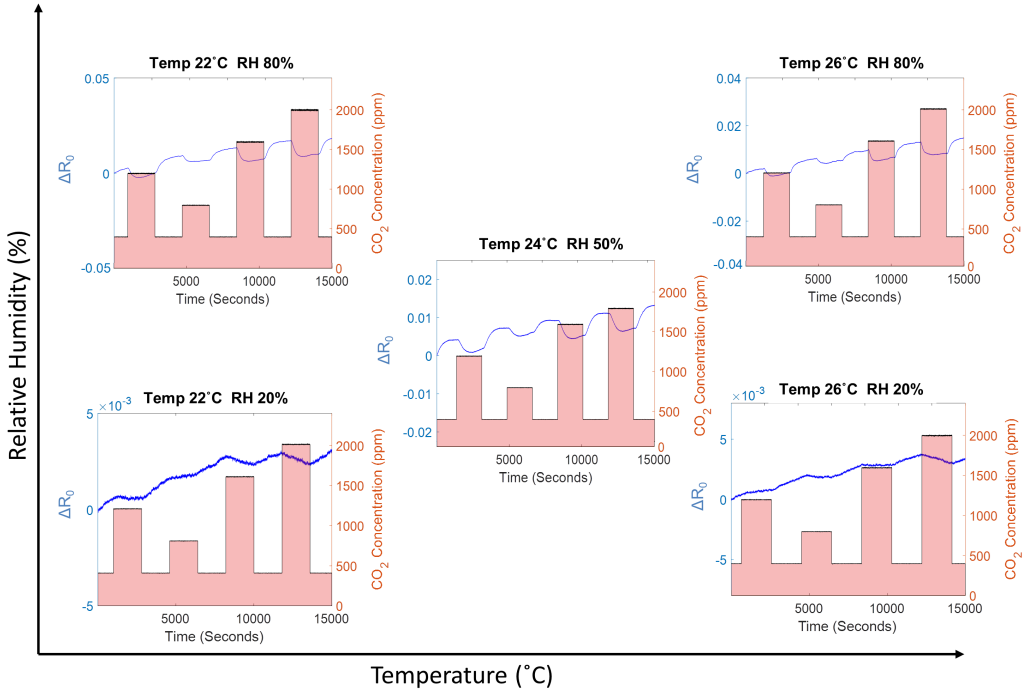

Figure 5: Time-series samples showing the change in resistance of the chemiresistive sensor at the "four corners and center" of the indoor comfort zone. This test zone spanned from approximately 22-26 °C and from dry air to 80% RH. The sensor response (blue line) is shown relative to changes in CO_2 concentration (red shaded regions).

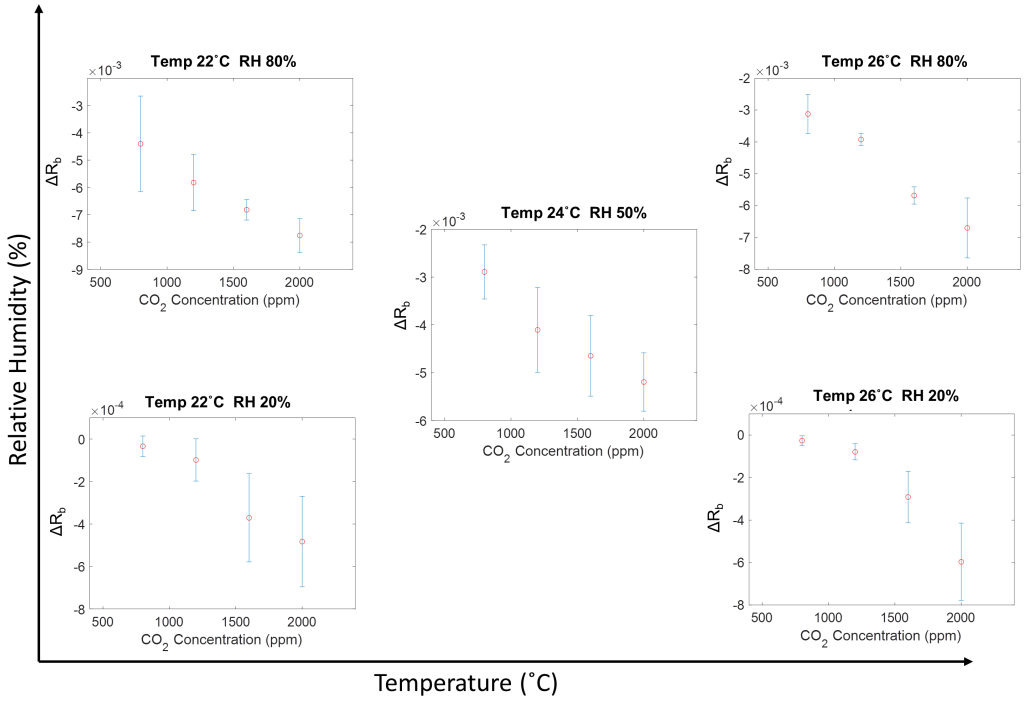

Figure 6: Chemiresistive sensor calibration curves at the "four corners and center" of the indoor comfort zone. The mean response at each CO_2 concentration is shown with error bars indicating one standard deviation in the data set.

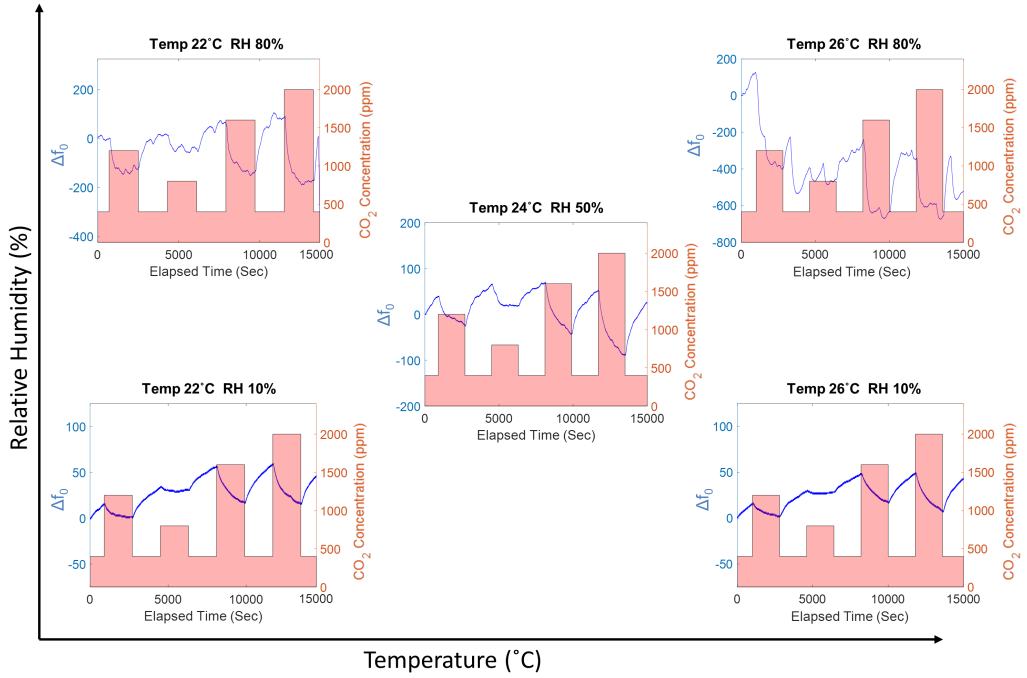

Figure 7: Time-series samples showing the frequency shift of the resonant mass sensor at the "four corners and center" of the indoor comfort zone. This test zone spanned from approximately 22-26 °C and from dry air to 80% RH. The sensor response (blue line) is shown relative to changes in CO_2 concentration (red shaded regions).

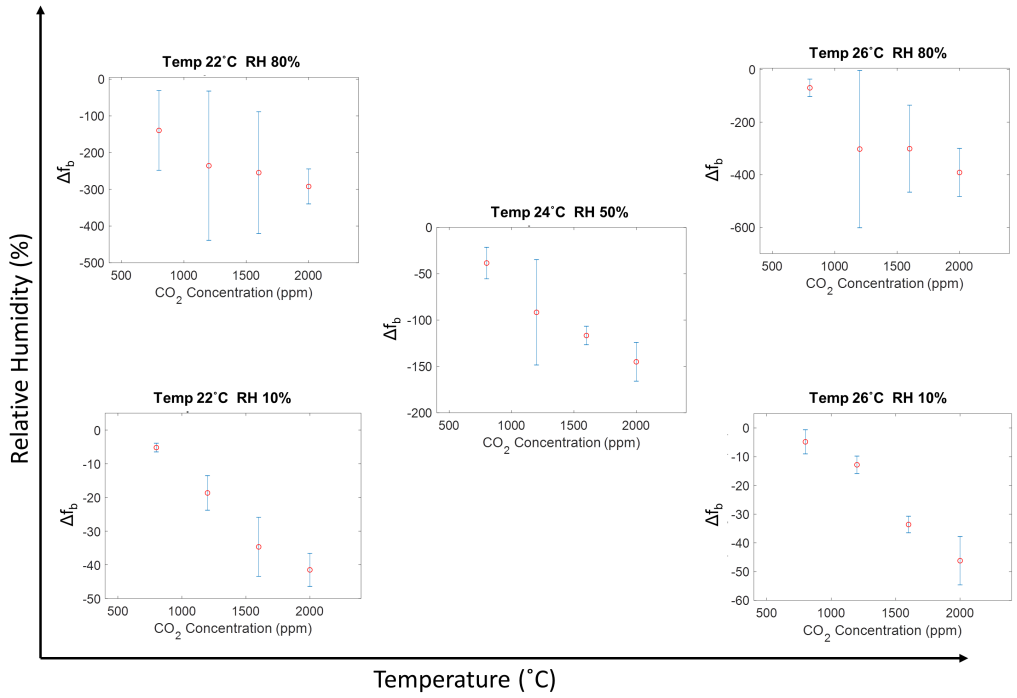

Figure 8: Resonant mass sensor calibration curves at the "four corners and center" of the indoor comfort zone. The mean response at each CO_2 concentration is shown with error bars indicating one standard deviation in the data set.

Similar to the chemiresistive sensor, the temperature range considered shows minor influence on the sensor. However, humidity plays a larger role. Though the magnitude of the sensor response is greater, the time-series signal clarity is reduced at high humidity levels. However, compared to the chemiresitistve device, the sensitivity of the resonant mass sensor is much higher at all of the considered environmental conditions, which is particularly important when a higher measurement resolution is necessary.

4.3 Comparison with Commercial Sensor Technologies

Commercially available low-cost CO_2 sensors include metal-oxide sensors (MOS) and most commonly nondispersive infrared (NDIR) sensors. Metal-oxide sensors can be utilized by measuring a change in resistance of a metal oxide film due to the adsorption of the target analyte. This change may result in an increase or decrease in resistance, depending on the target analyte and the sensing material being used. Metal-oxide sensors are a relatively low-cost option for CO_2 monitoring, however, accuracy below 2,000 ppm tends to be poor (Fine et al., 2010). NDIR sensors are most common for low-cost CO_2 monitoring below 2,000 ppm, such as in HVAC applications. NDIR sensors operate based on principles of molecular spectroscopy and their use in building applications, such as indoor air quality monitoring and demand-controlled ventilation have been demonstrated extensively (Labeodan et al., 2015; Emmerich & Persily, 2001; Yi et al., 2005; Schibuola et al., 2018; Ng et al., 2011). However, though still considered low-cost, these sensors typically market for $100-$200. As well, the infrared light inherent to NDIR sensors requires higher power consumption and a large sensor footprint, making them difficult to implement in embedded applications.

Comparatively, the power consumption of the chemiresistive and resonant mass sensors developed herein was relatively low in bench-top testing conditions. The chemiresistive devices were nominally 10 kΩ. For this range, the digital multimeter used for benchtop testing provides a load of about 100 μA; therefore, the chemiresistive devices in their current state require approximately 100 μW of power. During bench-top testing of the resonant mass sensors, each oscillator used about 18 mA when provided 3.3 V from a DC power supply. Therefore, the resonant mass sensors in their current state require approximately 60 mW of power. It is likely that the power consumption may be reduced if a commercial sensor package is realized and lab-grade measurements are no longer necessary. Even so, the chemiresistive and resonant mass CO_2 sensors consume far less power than typical commercial NDIR or MOS CO_2 sensors.

Table 1 provides a comparison of the prototype chemiresistive and resonant mass sensors, with typical commercial MOS and NDIR CO_2 sensors. For a comparable measurement range, the chemiresistive and resonant mass sensors are small, low-cost, and low-power. This is particularly important when considering wireless sensor deployment and high resolution indoor air monitoring. As such, these sensors are promising candidates for room-level CO_2 monitoring in both new and retrofit building applications.

Table 1: A comparision of prototype sensors with commercial sensing technologies

Sensor Type	Measurement Range	Footprint	Cost	Power
Chemiresistive	0-10,000 ppm	< 25 mm^2	<$50	100 μW
Resonant Mass	0-10,000 ppm	< 25 mm^2	<$50	60 mW
Metal-Oxide	2,000-10,000 ppm	< 25 mm^2	$50-$75	200 mW
Nondispersive infrared	0-10,000 ppm	3 cm^2	$100-$200	300 mW

5. CONCLUSIONS

Two novel CO_2 sensors utilizing a polymer blend of PEI and PEG were presented. The performance of prototype sensors in a bench-top environmental test system was demonstrated at CO_2 concentrations, temperatures, and humidity levels, typical of indoor conditions. A chemiresistive sensor utilizing CNTs and the polymer blend was shown to detect CO_2 with very low power consumption. Similarly, a resonant mass sensor, utilizing the polymer blend, was found to be more sensitive than its chemiresistive counterpart. However, this was achieved at the cost of slightly higher power consumption and reduced signal clarity at high humidity levels. Nevertheless, the power consumption and footprint of both of these sensors is much smaller than most of the commercial sensors currently available. Such metrics make wireless and ubiquitous CO_2 sensing in buildings relevant, which presents new opportunities in smart building controls.

With further development, these sensors may serve not only as an alternative to currently available commercial CO_2 sensors, but provide new data nodes throughout buildings that were previously not economically viable.

REFERENCES

ASHRAE. (2010a). *ASHRAE/ANSI Standard 55-2010 Thermal Environmental Conditions for Human Occupancy* (Tech. Rep.). Atlanta, GA: American Society of Heating, Refrigerating, and Air-Conditioning Engineers.

ASHRAE. (2010b). *ASHRAE/ANSI Standard 62.1-2010 Ventilation for Acceptable Indoor Air Quality* (Tech. Rep.). Atlanta, GA: American Society of Heating, Refrigerating, and Air-Conditioning Engineers.

Candanedo, L. M., & Feldheim, V. (2016). Accurate occupancy detection of an office room from light, temperature, humidity and CO_2 measurements using statistical learning models. *Energy and Buildings*, *112*, 28-39.

EIA. (2019). *Frequently Asked Questions on Buildings in the United States* (Report No. P-41). United States Energy Information Administration.

Ekwevugbe, T., Brown, N., Pakka, V., & Fan, D. (2013). Real-time building occupancy sensing using neural-network based sensor network. In *2013 7th IEEE International Conference on Digital Ecosystems and Technologies (DEST)* (p. 114-119).

Emmerich, S. J., & Persily, A. K. (2001). *State-of-the-Art Review of CO_2 Demand Controlled Ventilation Technology and Application* (Report No. 6729). NIST Interagency/Internal Report (NISTIR).

EPA. (1989). *Report to Congress on Indoor Air Quality* (Vol. 2; Report No. EPA/400/1-89/001C). United States Environmental Protection Agency.

Fine, G. F., Cavanagh, L. M., Afonja, A., & Binions, R. (2010). Metal oxide semi-conductor gas sensors in environmental monitoring. *Sensors*, *10*, 5469-5502.

Gunay, B., & Shen, W. (2017). Connected and distributed sensing in buildings: Improving operation and maintenance. *IEEE Systems, Man, and Cybernetics Magazine*, *3*, 27-34.

Jin, M., Bekiaris-Liberis, N., Weekly, K., Spanos, C. J., & Bayen, A. M. (2018). Occupancy detection via environmental sensing. *IEEE Transactions on Automation Science and Engineering*, *15*, 443-455.

Labeodan, T., Zeiler, W., Boxem, G., & Zhao, Y. (2015). Occupancy measurement in commercial office buildings for demand-driven control applications—a survey and detection system evaluation. *Energy and Buildings*, *93*, 303-314.

Li, X., Jung, Y., Sakimoto, K., Goh, T.-H., Reed, M. A., & Taylor, A. D. (2013). Improved efficiency of smooth and aligned single walled carbon nanotube/silicon hybrid solar cells. *Energy & Environmental Science*, *6*, 879-887.

Ng, L. C., & Wen, J. (2011). Estimating building airflow using CO_2 measurements from a distributed sensor network. *HVAC&R Research*, *17*, 344-365.

Ng, M. O., Qu, M., Zheng, P., Li, Z., & Hang, Y. (2011). CO_2-based demand controlled ventilation under new ASHRAE standard 62.1-2010: a case study for a gymnasium of an elementary school at West Lafayette, Indiana. *Energy and Buildings*, *43*, 3216-3225.

O'Neill, Z. D., Li, Y., Cheng, H. C., Zhou, X., & Taylor, S. T. (2020). Energy savings and ventilation performance from CO_2-based demand controlled ventilation: Simulation results from ASHRAE RP-1747 (ASHRAE RP-1747). *Science and Technology for the Built Environment*, *26*, 257-281.

Schibuola, L., Scarpa, M., & Tambani, C. (2018). CO_2 based ventilation control in energy retrofit: An experimental assessment. *Energy*, *143*, 606-614.

Yi, S., Park, Y., Han, S., Min, N., Kim, E., & Ahn, T. (2005). Novel NDIR CO_2 sensor for indoor air quality monitoring. In *The 13th International Conference on Solid-State Sensors, Actuators and Microsystems, 2005. Digest of Technical Papers. Transducers '05.* (Vol. 2, p. 1211-1214).

You, Y., Niu, C., Zhou, J., Liu, Y., Bai, Z., Zhang, J., … Zhang, N. (2012). Measurement of air exchange rates in different indoor environments using continuous CO_2 sensors. *Journal of Environmental Sciences*, *24*, 657-664.

ACKNOWLEDGMENT

The information, data, or work presented herein was funded in part by the Advanced Research Projects Agency-Energy (ARPA-E), U.S. Department of Energy, under Award Number DE-AR0000943. The views and opinions of authors expressed herein do not necessarily state or reflect those of the United States Government or any agency thereof.